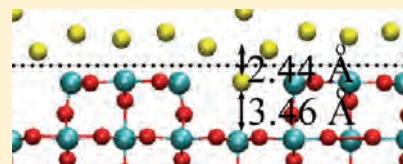


Au/TiO₂(110) Interfacial Reconstruction Stability from ab Initio

Min Yu[†] and Dallas R. Trinkle^{*‡}[†]Department of Physics, and [‡]Department of Materials Science and Engineering, University of Illinois at Urbana–Champaign, Urbana, Illinois 61801, United States

ABSTRACT: We determine the stability and properties of interfaces of low-index Au surfaces adhered to TiO₂(110), using density functional theory energy density calculations. We consider Au(100) and Au(111) epitaxies on rutile TiO₂(110) surface, as observed in experiments. For each epitaxy, we consider several different interfaces: Au(111)//TiO₂(110) and Au(100)//TiO₂(110), with and without bridging oxygen, Au(111) on 1 × 2 added-row TiO₂(110) reconstruction, and Au(111) on a proposed 1 × 2 TiO reconstruction. The density functional theory energy density method computes the energy changes on each of the atoms while forming the interface and evaluates the work of adhesion to determine the equilibrium interfacial structure.



INTRODUCTION

Bulk metallic Au is chemically inert and catalytically inactive as a consequence of combination of valence d orbitals and diffused valence s and p orbitals. Recently, Au nanoparticles have been found to be catalytically active when supported on metal oxides such as TiO₂, SiO₂, Fe₂O₃, Co₃O₄, NiO, Al₂O₃, MgO, etc.^{1–6} For example, Au nanoparticles supported on a TiO₂(110) surface demonstrate catalytic activity to promote the reaction between CO and O₂ to form CO₂ at $T < 40$ K with 3.5 nm Au nanoparticles maximizing activity.³ The catalytic activity is remarkably sensitive to the support material, Au particle size, and Au–support interaction; in addition, the reaction mechanism of CO oxidation over Au/TiO₂ system remains under debate.^{3,7–9} High-resolution transmission electron microscopy (HRTEM)^{10,11} and high-angle annular dark field scanning transmission electron microscopy (HAADF-STEM)^{11,12} have characterized the atomic structure of nanocrystal interface. However, the atomic structure of Au/TiO₂ interface is difficult to determine in HRTEM image simulations due to several issues, such as the thickness of nanoparticles and metal oxide substrates are not determined, the positions of atoms in the direction parallel to the electron beam are not determined, and the very low contrast for oxygen atoms. New HRTEM experiments¹¹ observed Au nanoparticles on TiO₂(110) surfaces with both the Au(111) and the Au(100) epitaxies, with the Au(111) epitaxy more frequently observed than Au(100). Their analysis with HAADF-STEM analyzed the reconstructed interface of epitaxial Au(111) sitting on a TiO₂(110) 1 × 2 surface and extracted important geometric information such as interlayer separations, the presence of Au in the interface of a 1 × 2 reconstruction, and estimates of the work of adhesion.

Density functional theory (DFT) calculations¹³ have studied the optimum size and stable adsorption of Au nanoparticles on rutile TiO₂(110). A single Au atom is energetically favorable on the site above 5-fold coordinated (5c) Ti atom on a stoichiometric TiO₂ surface¹⁴ and is most stable on the 2-fold coordinated (2c) bridging-O vacancy site on a reduced surface.^{15–17} Oxygen vacancies cause a stronger binding of Au atoms,¹⁸

nanoclusters,^{19–21} and nanorods²⁰ to the reduced TiO₂ surface than to the stoichiometric surface. Apart from the stoichiometric and reduced TiO₂ surfaces, Shi et al. found the O-rich interface is the most stable at low temperature of catalytic reaction after examining the Au-rod/TiO₂(110) in the orientation Au(111)//TiO₂(110) with different interface stoichiometry and various rigid-body translations.²² Recently, Shibata et al. examined two and nine Au(110) atomic layers supported on reduced TiO₂(110) and demonstrated that both the atomic and the electronic structure of two-layer Au are reconstructed, while the lattice coherency decays rapidly across the interface for nine-layer Au.²³ We compare different Au/TiO₂ interfaces: Au(111)//TiO₂(110) and Au(100)//TiO₂(110), with and without bridging oxygen, Au(111) on 1 × 2 added-row TiO₂(110) reconstruction,²⁴ and Au(111) on a new proposed 1 × 2 TiO reconstruction.¹¹ We use the newly reformulated^{25,26} density functional theory energy density method to evaluate energy for each atom in the interfacial reconstruction. This provides insight into interfacial stability from the changes in atomic energy from the formed interface and corrects for spurious errors in the work of adhesion from the remaining free surfaces in the computational cell. The new information of atomic energies extracted from density functional theory shows the response to bonding environment changes in interfaces. The comparison with experimental geometry¹¹ and work of adhesion²⁷ allows us to validate our predicted structures.

METHODOLOGY

We perform DFT calculations¹³ on the Au/TiO₂ interfaces using the projector augmented wave (PAW) method²⁸ with the Vienna ab initio simulation package (VASP).^{29,30} The exchange–correlation energy is treated in the Perdew–Burke–Ernzerhof³¹ version of the generalized gradient approximation functional (PBE-GGA). Elements Au, Ti, and O are given by [Xe]6s¹5d¹⁰, [Ne]3s²3p⁶4s²3d², and [He]2s²2p⁴ atomic configurations; this

Received: February 21, 2011

Revised: July 22, 2011

Published: August 01, 2011

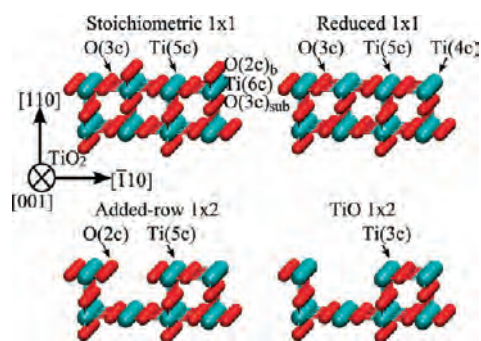


Figure 1. Geometry for four different $\text{TiO}_2(110)$ surface structures. Upper two are stoichiometric 1×1 and reduced 1×1 ; bottom two are added-row 1×2 reconstruction and $\text{TiO } 1 \times 2$ reconstruction. The stoichiometric structure has bridging oxygen ($2c$)_b atoms above the flat titanium ($5c$)/($6c$) and oxygen ($3c$) plane. Removal of the bridging oxygens produces a reduced surface, with 4- and 5-fold coordinated titanium. The added-row reconstruction removes every other row of Ti ($4c$) atoms with subsurface bridging oxygens ($3c$)_{sub} for a 1×2 reconstruction, with 2-fold coordinated oxygen. Finally, additional reduction of the added-row reconstruction, by removing the oxygen ($2c$) atoms neighboring the removed row, produces the TiO reconstruction with 3-fold coordinated titanium.

requires a plane-wave basis set cutoff at 900 eV. We use Monkhorst–Pack k -point meshes³² of $1 \times 6 \times 1$ for interface supercells; Brillouin-zone integration uses the Methfessel–Paxton method³³ with $k_B T = 0.2$ eV for electronic occupancies, and the total energy extrapolated to $k_B T = 0$ eV. The calculated lattice constant for Au in the FCC phase is 4.171 Å, and for TiO_2 the rutile phase $a = 4.649$ Å, $c = 2.970$ Å, and $u = 0.305$. These calculated values compare well with the experimental values of 4.08 Å for Au and $a = 4.584$ Å, $c = 2.953$ Å, $u = 0.305$ ⁶ for TiO_2 .

The work of adhesion of forming an interface from two individual surfaces can be determined from total energy calculations:

$$E_{\text{adh}} = \frac{1}{A}(E_{\text{Au}} + E_{\text{TiO}_2} - E_{\text{Au/TiO}_2}) \quad (1)$$

where E_{Au} and E_{TiO_2} are the energy of relaxed Au surface and relaxed TiO_2 surface, and $E_{\text{Au/TiO}_2}$ is the energy of the interface system. To avoid differences in grid densities or the planewave basis, the surfaces are computed with the same supercell as the interface system. In addition to total energies, the energy density method proposed by Chetty and Martin²⁵ provides the formation energy for more than one surface or interface in one calculation, and a picture of the distribution of energy among the surrounding atoms. We use a new reformulation of the energy density method for the PAW method.²⁶ Moreover, we compute atomic energies by integrating the local energy density over gauge-independent integration volumes.³⁴ The data allow us to identify the spatial range of the interface and give insight into the nature of interfacial stability. The integration of the energy density over these volumes produces a small integration error, which can be estimated from the extent to which gauge-invariance is broken; we include that error as a \pm range in all of our reported energy density calculations. For the Au/ TiO_2 interfaces, the supercell configurations in the calculations are periodic parallel to the interface and contain six layers of Au, eight trilayers of TiO_2 , and 10.5 Å vacuum region. Because of the lattice mismatch, Au layers are strained to lattice match the TiO_2 according to the supercell periodicity; strained Au surfaces are used as references for energy differences. Atomic relaxation is

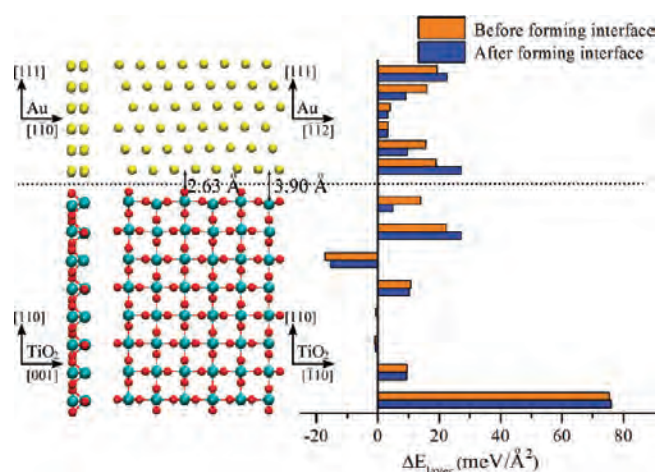


Figure 2. Geometry and energy of Au(111) on the stoichiometric $\text{TiO}_2(110)$ surface following relaxation. The atomic energy on each layer is referenced to the bulk and is shown before (orange) and after (blue) forming the interface. The interfacial distance relaxes to 3.90 Å between Au and Ti layers, and to 2.63 Å between Au and bridging-O layers.

allowed for all six layer Au atoms and for three interfacial layers of TiO_2 for all geometries considered. In addition, different translations of Au relative to TiO_2 are attempted to determine the minimum energy configuration. The equilibrium positions of the atoms are determined by requiring the force on each relaxed atom to be smaller than 0.02 eV/Å.

■ INTERFACES

Figure 1 shows the four different configurations of rutile $\text{TiO}_2(110)$ substrates we consider. We start with a stoichiometric surface and then reduce the surface by removing all bridging-O atoms; both are 1×1 surfaces. Pang et al. proposed an added-row 1×2 reconstruction for the rutile (110) surface, where one row of Ti atom with its sub-bridging-O row is removed per 1×2 cell for a fully reduced surface.²⁴ Finally, removing the 2-fold coordinated O atoms from the added-row reconstruction gives a TiO reconstruction. While this reconstruction is not the lowest in energy, it provides the most stable Au/ TiO_2 interface that also matches the experimentally observed geometry.

Au(111)/ $\text{TiO}_2(110) 1 \times 1$: Stoichiometric and Reduced Interfaces. Both interfaces on 1×1 surfaces use a similar geometry for relaxation. Along the direction Au[$1\bar{1}0$]/ TiO_2 -[001], a single repeat length of Au and TiO_2 gives a 1% lattice mismatch. This agrees with STEM measurements showing registry even up to 10 layers from the interface.¹¹ Along the direction Au[$1\bar{1}2$]/ TiO_2 [$\bar{1}10$], a repeat length of 4 for Au matches with a repeat length of 3 for TiO_2 , producing a total 3.6% lattice mismatch strain at the interface. The supercells contain 48 Au, 48 Ti, and 96 O atoms in the interface configuration with stoichiometric TiO_2 surface, and 3 fewer O atoms for the reduced TiO_2 surface. After relaxation, we determine the interlayer spacing at the interface; with energy density calculations, we can ignore any spurious energy changes due to the opposing Au and TiO_2 surfaces.

Figures 2 and 3 show the geometry of the relaxed Au(111) on stoichiometric and reduced $\text{TiO}_2(110)$ surfaces. The interfacial distance between Au and Ti layers relaxed to 3.90 Å with stoichiometric TiO_2 surface, and 2.79 Å in the configuration with reduced TiO_2 surface. From total energy, the work of

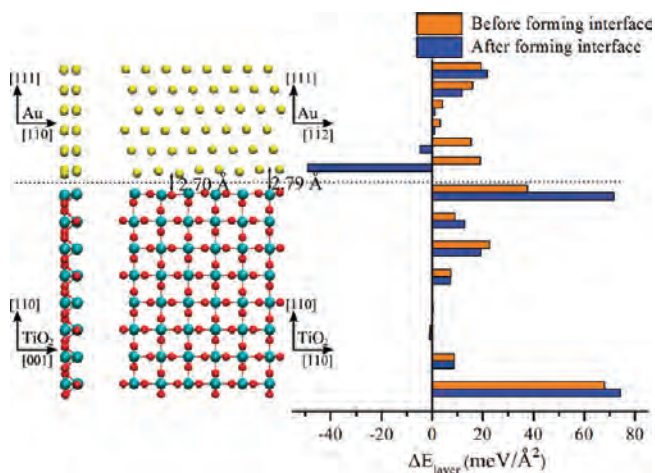


Figure 3. Geometry and energy of Au(111) on the reduced TiO₂(110) surface following relaxation. Energy per layer in the reference of bulk value is given before (orange) and after (blue) forming the interface. The interfacial distance relaxes to 2.79 Å between Au and Ti layers, and to 2.70 Å between Au and in-plane O layers. The geometry reduces the energy of the surface Au layer to a more stable configuration than that of the stoichiometric TiO₂ surface.

adhesion of the interface with stoichiometric TiO₂ surface is 7 meV/Å², while the work of adhesion of the interface with the reduced TiO₂ surface is 54 meV/Å². The differences in interlayer spacing and energy are due to the presence or absence of bridging oxygen atoms on the TiO₂ surface. Energy density shows that TiO₂ layers reach bulk behavior by the fifth layer from the interface. We integrate the energy density over two Au layers and four TiO₂ layers to evaluate the work of adhesion strictly from changes in energy near the interface. This gives a work of adhesion of 4 ± 1 meV/Å² to the stoichiometric TiO₂ surface, and 53 ± 1 meV/Å² to the reduced TiO₂ surface. The work of adhesion is primarily due to a decrease in energy of the Au surface layer at the reduced TiO₂ surface. This suggests that the main effect of removing bridging oxygen is to provide a flat surface for Au(111) layers to adhere, and that the TiO₂ surface energy change is significantly less than the Au surface energy change.

Au(111)/TiO₂(110) 1 × 2: Added-Row and TiO Reconstruction. Both interfacial reconstructions on 1 × 2 surfaces use a similar geometry for relaxation. Along the direction Au[1 $\bar{1}$ 0]/TiO₂[001], a single repeat length of Au and TiO₂ gives a 1% lattice mismatch as for the 1 × 1 reconstructions. Along the direction Au[$\bar{1}$ 12]/TiO₂[$\bar{1}$ 10], a repeat length of 5 for Au matches with a repeat length of 4 for TiO₂, producing a total 2.9% lattice mismatch strain at the interface; the different periodicity is required for a 1 × 2 reconstruction. The supercells contain 62 Au, 62 Ti, and 122 O atoms in the interface configuration with added-row TiO₂ reconstruction, and 4 fewer O atoms for the TiO reconstruction. After relaxation, we determine the interlayer spacing at the interface; with energy density calculations, we can ignore any spurious energy changes due to the opposing Au and TiO₂ surfaces.

Added-Row Reconstruction. The added-row reconstruction for the 1 × 2 rutile (110) surface removes one row of Ti atom with its sub-bridging-O row per 1 × 2 cell for a fully reduced surface.²⁴ Experimental observations of the interface find a mixed TiO₂–Au layer with 1 × 2 periodicity;¹¹ to build our interface and compute the work of adhesion, we consider

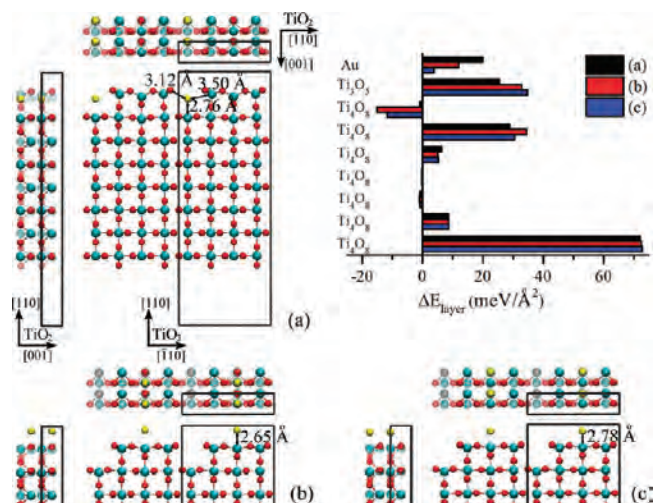


Figure 4. Three different configurations of a single Au row on the TiO₂ added-row reconstruction: (a) in the missing Ti row with 4 nearest neighboring O atoms; (b) on top of the TiO₂ surface directly above a Ti atom; (c) on top of the TiO₂ surface bridging between two Ti atoms. Au atoms are in gold, and the wireframe shows the supercell. Opaque atoms are on the top layer, while transparent atoms are on lower layers. The (c) configuration has the lowest total energy, 6.3 meV/Å² lower than the (b) configuration, and 15.7 meV/Å² lower than the (a) configuration. From the energy calculations, the Au row controls the total energy, with the largest increase in energy from filling the missing Ti–O row in the surface layer; hence, we expect to see a mixing of the TiO₂ surface with Au only after coverage by a gold nanoparticle.

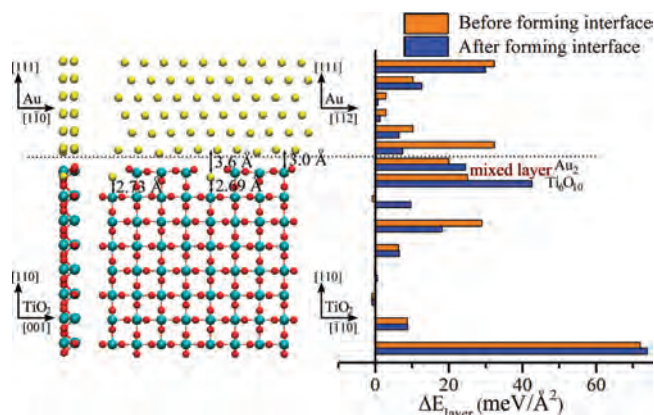


Figure 5. Geometry and energy of the Au(111)/TiO₂ added-row reconstruction following relaxation. Atomic energy per layer in the reference of bulk value is given before (orange) and after (blue) forming the interface. The interfacial distance between Au layer with mixed layer is about 3.4 Å, and the work of adhesion is -9 meV/Å². While the Au surface layer reduces its energy, the TiO₂ layer increases in energy as the oxygen atoms that neighbor the in-surface Au rows are unable to relax out of the (110) plane; hence, the Ti₆O₁₀ layer increases in energy.

different configurations to attach a row of Au atoms on added-row reconstruction in Figure 4. After geometry relaxation, the configuration of each Au atom sitting on the top of two Ti atoms with 4 neighboring O atoms is the most stable; there is an energy cost of 15.7 meV/Å² to place a Au row into the missing row of TiO₂. This is similar to the adhesion of Au rows to bridging oxygen vacancies in a TiO₂(110) “missing row”

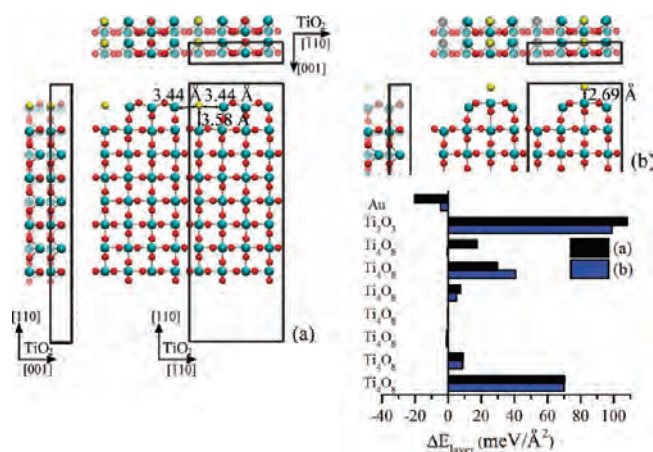


Figure 6. Two different configurations of a single Au row on the TiO reconstruction: (a) in the missing Ti row; (b) on top of the TiO₂ surface bridging between two Ti atoms. Au atoms are in gold, and the wire-frame shows the supercell. Opaque atoms are on the top layer, while transparent atoms are on lower layers. The energy of the (b) configuration is 0.8 meV/Å² lower than that of the (a) configuration. Adding Au into the missing row only slightly increases the energy of the Au row; this increase is much less than for the TiO₂ added-row reconstruction. However, the TiO reconstruction is a higher energy surface than the added-row reconstruction.

reconstruction.²⁰ The energy density shows that the energy of Au dominates the stability.

Figure 5 shows the geometry of the relaxed Au(111) on added-row TiO₂ reconstruction. The interfacial distance between Au and the mixed interfacial layer is 3.4 Å. This larger distance is due to the displacement of oxygen atoms neighboring the interfacial Au rows. From total energy, the work of adhesion of the interface is -9 meV/Å² after accounting for the 16 meV/Å² increase in energy due to the addition of Au into the subsurface (cf., Figure 4). We integrate the energy density over two Au interfacial layers, one mixed interfacial layer, and three next TiO₂ interfacial layers and subtract the corresponding energy density integration in Au layers and the ground-state configuration of an Au row on TiO₂, Figure 4a. This energy density calculation gives a work of adhesion of 6 ± 1 meV/Å² before subtracting 16 meV/Å². After forming the interface, the atomic energy of Au interfacial layer drops, while the atomic energy of TiO₂ in the mixed layer increases. The increase in the energy of the surface Ti₆O₁₀ layer is due to the constraint placed on oxygen atoms neighboring to the intermixed Au row in the mixed layer.

TiO Reconstruction. The added-row reconstruction can be further reduced by removing the 2-fold coordinated O atoms on the TiO₂ surface layer to form a TiO 1×2 reconstruction. This reconstruction is suggested by the energy density calculations above as a possible route to increase the work of adhesion. We build our interface in a manner similar to that for the added-row reconstruction and consider different configurations to attach one row of Au atoms on the reconstruction in Figure 6. After geometry relaxation, both the Au row in the missing row of Ti and on the surface have large, but similar, energies (a difference of 0.8 meV/Å²). The increase in surface energy is entirely due to the first TiO₂ layer, suggesting that further reduction to TiO is unfavorable without an interfacial layer of gold to “protect” the surface.

Figure 7 shows the geometry of the relaxed Au(111)//TiO reconstruction interface. Despite the higher energy of the TiO

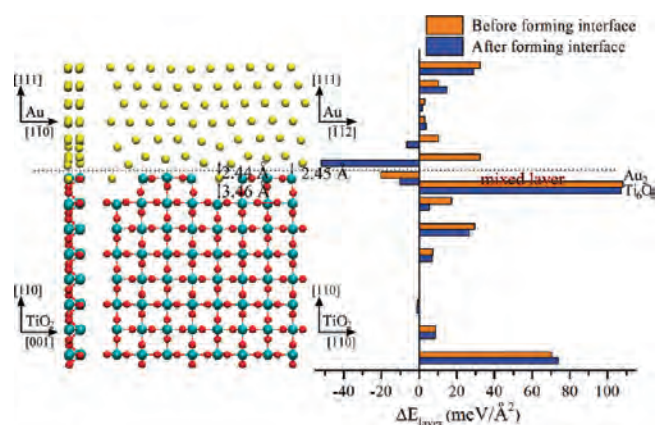


Figure 7. Geometry and energy of the Au(111)//TiO reconstruction following relaxation. Atomic energy per layer in the reference of bulk value is given before (orange) and after (blue) forming the interface. The interfacial distance between Au layer with mixed layer is 2.45 Å, as compared to the experimental observation of 2.35 ± 0.16 Å. The work of adhesion is 107 meV/Å² from energy density integration as compared to the Au(111) and TiO reconstruction filled with a Au row. The stability of the interface comes from a reduction in the Au surface energy with no penalty in the mixed layer, as occurs with the added-row reconstruction.

reconstruction, it produces an attractive interface configuration with Au(111). The interfacial distance between the Au layer and mixed interfacial layer is 2.44–2.45 Å; the closer attachment distance as compared to the added-row reconstruction is due to the removed oxygen atoms in the interfacial layer. From total energy, the work of adhesion of the interface is 99 meV/Å². We integrate the energy density over two Au interfacial layers, one mixed interfacial layer, and three next TiO₂ interfacial layers and subtract the corresponding energy density integration in Au layers and the ground-state configuration of an Au row on TiO, Figure 6a. This energy density calculation gives a work of adhesion of 107 ± 1 meV/Å²; the difference with the total energy calculation is due to spurious changes in the free TiO₂ surface that the energy density calculation removes. We observe a remarkable drop of atomic energy of Au at the interfacial layer. In addition, the mixed layer energy sees only a small change leading to a stabilized interface. To compute the true work of adhesion, however, we must account for the energy change due to a further reduction from the added-row reconstruction to the TiO reconstruction.

Figure 8 shows the changes in local electronic density of states for atoms in the Au(111)//TiO interface as compared to other atomic configurations in Au and TiO₂. In the interface, the Au atom mixed in the TiO₂ layer has a narrower width, indicating reduced bonding to neighbors than Au atoms in the interfacial layer above. Moreover, the Au d states are pushed toward the Fermi level, even compared to atoms on a free surface. The widening of the density of states for Au atoms in the interface as compared to the free surface corresponds to changes in atomic energy in Figure 7. Titanium has a downward shift in unoccupied states pulling them below the Fermi energy in the interface. Finally, the oxygen atom in the surface next to Au (cf., Figure 5) that is removed in the new reconstruction sees its density of states narrow and produce a peak; this increase in energy corresponds to the atomic energy changes also seen for this atom. After removal, the remaining oxygen neighbors have bonding environments that are less disturbed by the presence of Au in the interfacial layer.

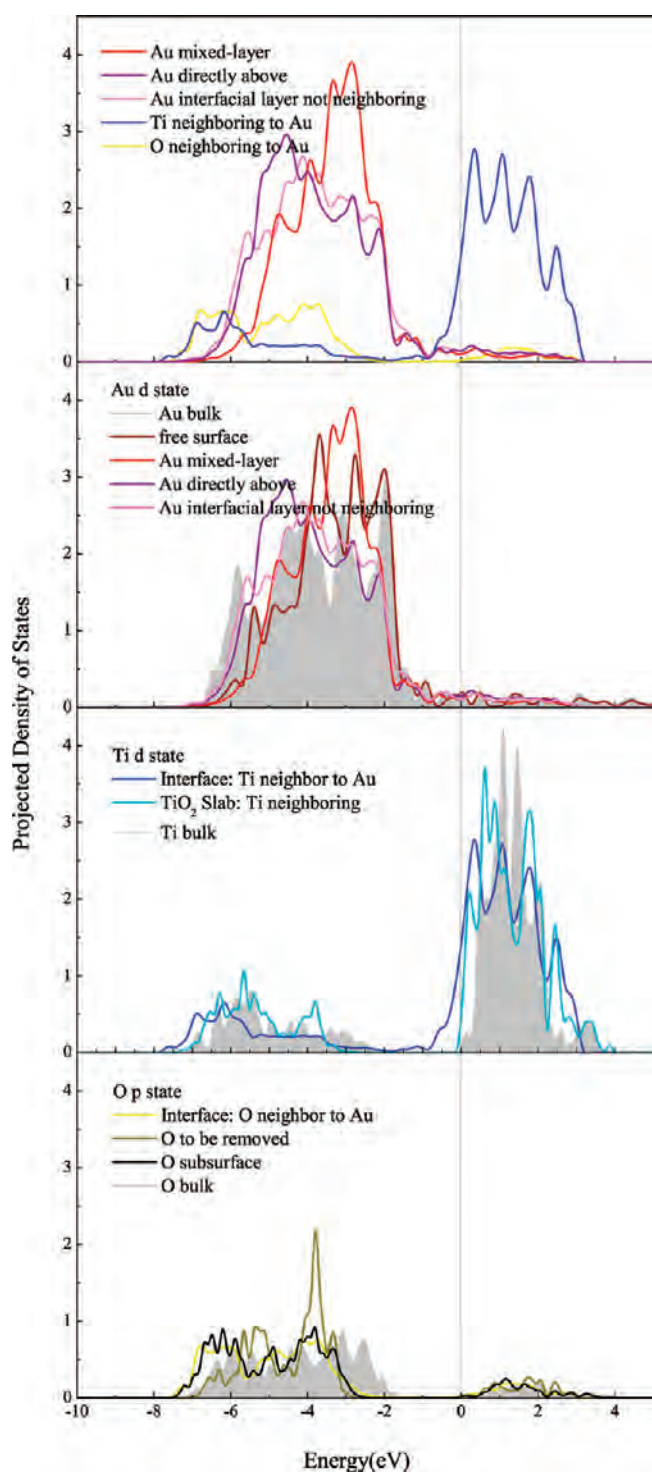


Figure 8. The projected density of states for Au, Ti, and O in the relaxed Au(111)//TiO₂ reconstruction. The top panel shows three types of Au atoms – in the mixed layer, in the interfacial layer neighboring or not neighboring to mixed-layer Au – and Ti and O atoms that neighbor Au in the mixed-layer. The following panels compare Au-5d, Ti-3d, O-2p DOSs in the relaxed Au(111)//TiO₂ reconstruction to other atomic environments: 5d states for Au bulk and (111) free surface; 3d states for Ti neighboring to missing row in 1 × 2 TiO₂ added-row reconstruction and Ti bulk; 2p states for O to be removed and O subsurface atoms in added-row reconstruction and O bulk.

Work of Adhesion. Figure 9 shows the relative energies for the different configurations to produce the two different 1 × 2

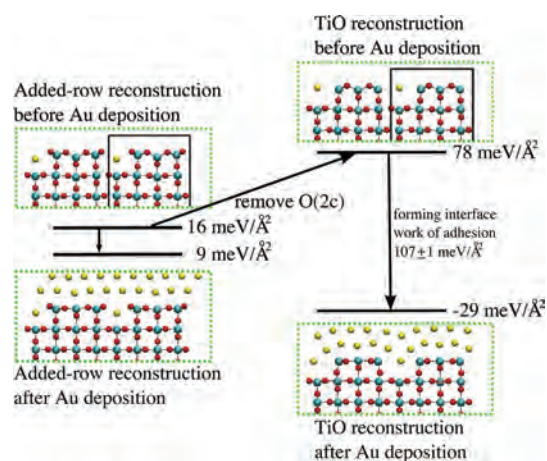


Figure 9. Evaluation of work of adhesion for Au(111) on 1 × 2 TiO₂(110) reconstructions. The top two energies are changes in the surface energy before the interface is formed and are relative to the stable 1 × 2 TiO₂(110) added-row reconstruction; hence, we start by adding 16 meV/Å² when Au is added into the surface (cf., Figure 4). The bottom two energies are relative to the Au(111) surface and the TiO₂(110) surface, the negative work of adhesion. The TiO reconstruction leads to a stable interface after Au deposition as the energy required to remove additional oxygen atoms from the added-row reconstruction is offset by a larger reduction in energy when forming the interface. This is an interesting example of an interfacial reconstruction that is stabilized solely in the presence of the interface. As compared to the other simple added-row reconstruction, which produces a small work of adhesion due to distortions in the mixed layer, the TiO interfacial reconstruction explains the observed 1 × 2 reconstruction, the interlayer spacing, and is energetically favorable.

reconstructions of Au(111)//TiO₂(110). Au(111) adhered to the TiO reconstruction is the most stable interface configuration with an interfacial distance 2.45 Å that agrees with the STEM observed,¹¹ 2.35 ± 0.16 Å. However, the work of adhesion of 107 meV/Å² is relative to the higher energy TiO surface with the introduced Au into the subsurface. The difference between the added-row reconstruction and the TiO reconstruction means that a single Au row on the TiO reconstruction is less stable by 62 meV/Å², plus 16 meV/Å² to place Au in the subsurface (cf., Figure 4); hence, the TiO reconstruction produces a stable configuration with work of adhesion of 29 meV/Å² after Au deposition. Note that we have computed our work of adhesion relative to the strained Au(111) surface with energy 38 ± 1 meV/Å² (43 meV/Å² for the unstrained surface) and the 1 × 2 added-row reconstruction for TiO₂(110) with an energy of 80 ± 1 meV/Å². This is lower than simply adhering to the added-row reconstruction, which has a work of adhesion of −9 meV/Å². It should be noted that the intermediate configuration of TiO without Au(111) is unstable and is needed to compute relative energies; given the higher surface energy, it is unlikely that further oxygen reduction occurs before the growth of Au(111) layers.

Au(100)//TiO₂(110) 1 × 1: Stoichiometric and Reduced Interfaces. Both interfaces on 1 × 1 surfaces use a similar geometry for relaxation. Along the direction Au[01 $\bar{1}$]/TiO₂-[001], a single repeat length of Au and TiO₂ gives a 1% lattice mismatch. Along the direction Au[011]/TiO₂[$\bar{1}$ 10], a repeat length of 9 for Au matches with a repeat length of 4 for TiO₂, producing a 0.9% lattice mismatch. The supercell contains 54 Au, 64 Ti, and 128 O atoms for the stoichiometric case, and 4 fewer O atoms for the reduced case. As before, we determine the

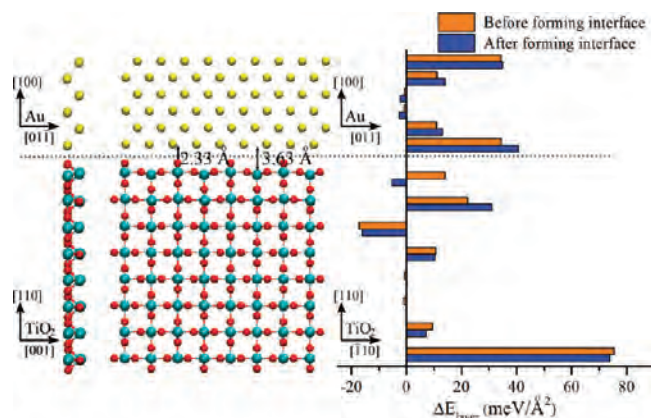


Figure 10. Geometry and energy of Au(100) on the stoichiometric $\text{TiO}_2(110)$ surface following relaxation. The atomic energy on each layer is referenced to the bulk and is shown before (orange) and after (blue) forming the interface. The interfacial distance is 3.63 Å between Au and Ti layers, and 2.33 Å between Au and bridging-O layers.

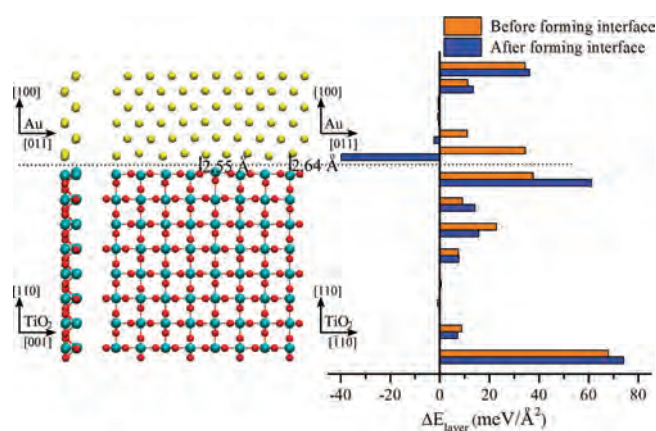


Figure 11. Geometry and energy of Au(100) on the reduced $\text{TiO}_2(110)$ surface following relaxation. The atomic energy on each layer is referenced to the bulk and is shown before (orange) and after (blue) forming the interface. The interfacial distance is 2.64 Å between Au and Ti layers, and 2.55 Å between Au and in-plane O layers. The Au layer energy is reduced, while the TiO_2 layer energy increases for a work of adhesion of $64 \pm 1 \text{ meV}/\text{Å}^2$.

interlayer spacing at the interface following relaxation; with energy density calculations, we can ignore any spurious energy changes due to the opposing Au and TiO_2 surfaces.

Figures 10 and 11 show the geometry of the relaxed Au(100) on stoichiometric and reduced $\text{TiO}_2(110)$ surfaces. The interfacial distance between Au and Ti layers relaxed to 3.63 Å with stoichiometric TiO_2 surface, and 2.64 Å in the configuration with reduced TiO_2 surface. From total energy, the work of adhesion is $3 \text{ meV}/\text{Å}^2$ of the interface with stoichiometric, while the work of adhesion of the interface with the reduced TiO_2 surface is $55 \text{ meV}/\text{Å}^2$. The differences in interlayer spacing and energy are due to the presence or absence of bridging oxygen atoms on the TiO_2 surface. Energy density shows that TiO_2 layers reach bulk behavior by the fifth layer from interfaces. We integrate the energy density over two Au layers and four TiO_2 layers to evaluate the work of adhesion strictly from changes in energy near the interface. This gives a work of adhesion of $1 \pm 1 \text{ meV}/\text{Å}^2$ to the stoichiometric TiO_2 surface, and $64 \pm 1 \text{ meV}/\text{Å}^2$ to the

Table 1. Comparison of Different Au(111)// $\text{TiO}_2(110)$ Interfaces^a

	E_{adh} [$\text{meV}/\text{Å}^2$]	$d_{\text{Au-Ti}}$ [Å]	misfit	
stoichiometric	1×1	$7 4 \pm 1$	3.90	3.6%
reduced	1×1	$54 53 \pm 1$	2.79	3.6%
added-row	1×2	$-9 -9 \pm 1$	3.00	2.9%
TiO	1×2	$22 29 \pm 1$	2.45	2.9%
experiment ^{11,27}	1×2	28 ± 7	2.35 ± 0.16	

^aThe two different work of adhesion values are from the total energy calculation of eq 1 and the energy density integration; the latter accounts for finite-size errors in the supercell calculation. The Au(111)// TiO_2 reconstruction agrees with experimental observation in three factors: the 1×2 symmetry, the work of adhesion E_{adh} , and the Au–Ti separation distance $d_{\text{Au-Ti}}$. The work of adhesion $29 \pm 1 \text{ meV}/\text{Å}^2$ compares well with $28 \pm 7 \text{ meV}/\text{Å}^2$; the experimental value²⁷ comes from the Wulff–Kaisew theorem³⁵ where $\Delta h/h = E_{\text{adh}}/\gamma_{\text{Au}(111)}$, and the geometry parameter $\Delta h/h$ characterizes various equilibrium shapes of supported Au nanoparticles in experiments. The surface energy $\gamma_{\text{Au}(111)}$ is $43 \text{ meV}/\text{Å}^2$ from our PAW-GGA-PBE calculation.

reduced TiO_2 surface. Similar to the Au(111)// $\text{TiO}_2(110)$ reduced interface, atomic energy at the interface decreases in the Au surface, and increases in the TiO_2 surface in the reduced case when forming the interface, to stabilize the structure more than the stoichiometric case. The energy of TiO_2 free surface away from the interface experiences a spurious energy change during the interface formation. Therefore, the integration of energy density over interfacial region reduces the finite-size error and provides more accurate work of adhesion or interfacial energy.

CONCLUSIONS

Table 1 summarizes the geometric and energy comparison of proposed Au(111)// $\text{TiO}_2(110)$ interfaces and the experimental observations.^{11,27} Density functional theory energy density calculations of several Au/ TiO_2 interfacial reconstructions determine the equilibrium structure that matches experimental measurements. Both Au(111) and (100) prefer attaching to reduced rutile (110) surfaces over stoichiometric surfaces. Comparison of Au(111) attaching on two $\text{TiO}_2(110)$ 1×2 reconstruction cells shows that the TiO reconstruction leads to the most stable interface configuration with interfacial distance 2.45 Å, and work of adhesion $29 \text{ meV}/\text{Å}^2$. Atomic energy variation during interface formation demonstrates that the attraction of top Au interfacial layer leads to a stable structure. The energy density computation also identifies spurious changes to atomic energies on the free-surfaces during the formation of an interface, which affect the computation of work of adhesion from total energy calculations; these finite-size errors are removed. Our calculations provide an atomistic-level explanation of the stability of the unusual TiO reconstruction, where further reduction of the interface is possible when “protected” by an epitaxial gold layer and demonstrates the power of energy density computation to guide the identification of stable defect structures.

AUTHOR INFORMATION

Corresponding Author

*E-mail: dtrinkle@illinois.edu.

ACKNOWLEDGMENT

This research was supported by the NSF under grant number DMR-1006077 and through the Materials Computation Center at UIUC, NSF DMR-0325939, and with computational resources from NSF/TeraGrid provided by NCSA and TACC. We thank J. M. Zuo and S. Sivaramkrishnan for discussion of the experimental results, and R. M. Martin for helpful discussions.

REFERENCES

- (1) Haruta, M.; Kobayashi, T.; Sano, H.; Yamada, N. *Chem. Lett.* **1987**, *2*, 405.
- (2) Haruta, M.; Yamada, N.; Kobayashi, T.; Iijima, S. *J. Catal.* **1989**, *115*, 301.
- (3) Valden, M.; Lai, X.; Goodman, D. W. *Science* **1998**, *281*, 1647.
- (4) Bocuzzi, F.; Chiorino, A.; Manzoli, M.; Andreeva, D.; Tabakova, T. *J. Catal.* **1999**, *188*, 176.
- (5) Hayashi, T.; Tanaka, K.; Haruta, M. *J. Catal.* **1998**, *178*, 566.
- (6) Diebold, U. *Surf. Sci. Rep.* **2003**, *48*, 53.
- (7) Bond, G. C.; Thompson, D. T. *Gold Bull.* **2000**, *33*, 41.
- (8) Grunwaldt, J.-D.; Maciejewski, M.; Becker, O.; Fabrizioli, P.; Baiker, A. *J. Catal.* **1999**, *186*, 458.
- (9) Haruta, M. *Gold Bull.* **2004**, *37*, 27.
- (10) Cosandey, F.; Madey, T. E. *Surf. Rev. Lett.* **2001**, *8*, 73.
- (11) Sivaramkrishnan, S.; Yu, M.; Pierce, B. J.; Scarpelli, M. E.; Wen, J.; Trinkle, D. R.; Zuo, J.-M. under review.
- (12) Akita, T.; Tanaka, K.; Kohyama, M.; Haruta, M. *Surf. Interface Anal.* **2008**, *40*, 1760.
- (13) Kohn, W.; Sham, L. J. *Phys. Rev.* **1965**, *140*, A1133.
- (14) Yang, Z.; Wu, R.; Goodman, D. W. *Phys. Rev. B* **2000**, *61*, 14066.
- (15) Wang, Y.; Hwang, G. S. *Surf. Sci.* **2003**, *542*, 72.
- (16) Amrendra, V.; Greg, M.; Horia, M. *J. Chem. Phys.* **2003**, *118*, 6536.
- (17) Wahlström, E.; Lopez, N.; Schaub, R.; Thostrup, P.; Rønnow, A.; Africh, C.; Lægsgaard, E.; Nørskov, J. K.; Besenbacher, F. *Phys. Rev. Lett.* **2003**, *90*, 026101.
- (18) Okazaki, K.; Morikawa, Y.; Tanaka, S.; Tanaka, K.; Kohyama, M. *Phys. Rev. B* **2004**, *69*, 235404.
- (19) Lopez, N.; Nørskov, J. K.; Janssens, T. V. W.; Carlsson, A.; Puig-Molina, A.; Clausen, B. S.; Grunwaldt, J.-D. *J. Catal.* **2004**, *225*, 86.
- (20) Pabisiak, T.; Kiejna, A. *Phys. Rev. B* **2009**, *79*, 085411.
- (21) Pillay, D.; Hwang, G. S. *Phys. Rev. B* **2005**, *72*, 205422.
- (22) Shi, H.; Kohyama, M.; Tanaka, S.; Takeda, S. *Phys. Rev. B* **2009**, *80*, 155413.
- (23) Shibata, N.; Goto, A.; Matsunaga, K.; Mizoguchi, T.; Findlay, S. D.; Yamamoto, T.; Ikuhara, Y. *Phys. Rev. Lett.* **2009**, *102*, 136105.
- (24) Pang, C. L.; Haycock, S. A.; Raza, H.; Murray, P. W.; Thornton, G.; Gülseren, O.; James, R.; Bullett, D. W. *Phys. Rev. B* **1998**, *58*, 1586.
- (25) Chetty, N.; Martin, R. M. *Phys. Rev. B* **1992**, *45*, 6074.
- (26) Yu, M.; Trinkle, D. R.; Martin, R. M. *Phys. Rev. B* **2011**, *83*, 115113.
- (27) Sivaramkrishnan, S.; Wen, J.; Scarpelli, M. E.; Pierce, B. J.; Zuo, J.-M. *Phys. Rev. B* **2010**, *82*, 195421.
- (28) Blöchl, P. E. *Phys. Rev. B* **1994**, *50*, 17953.
- (29) Kresse, G.; Furthmüller, J. *Phys. Rev. B* **1996**, *54*, 11169.
- (30) Kresse, G.; Joubert, D. *Phys. Rev. B* **1999**, *59*, 1758.
- (31) Perdew, J. P.; Burke, K.; Ernzerhof, M. *Phys. Rev. Lett.* **1996**, *77*, 3865.
- (32) Monkhorst, H. J.; Pack, J. D. *Phys. Rev. B* **1976**, *13*, 5188.
- (33) Methfessel, M.; Paxton, A. T. *Phys. Rev. B* **1989**, *40*, 3616.
- (34) Yu, M.; Trinkle, D. R. *J. Chem. Phys.* **2011**, *134*, 064111.
- (35) Winterbottom, W. L. *Acta Metall.* **1967**, *15*, 303.